A Comprehensive Three-Dimensional Model for Simulation of Combustion Systems: PCGC-3

Presented By:

Andrew Eaton

Scott C. Hill
L. Douglas Smoot

Advanced Combustion Engineering Research Center
Brigham Young University

Reprinted from ENERGY & FUELS, 1993, 7.

A Comprehensive Three-Dimensional Model for Simulation of Combustion Systems: PCGC-3

Scott C. Hill*,† and L. Douglas Smoot‡

Advanced Combustion Engineering Research Center, 75 CTB, Brigham Young University, Provo, Utah 84602

Received May 21, 1993. Revised Manuscript Received September 8, 1993•

A generalized, three-dimensional combustion model has been developed to simulate large-scale, steady-state, gaseous and particle-laden, reacting and nonreacting systems. The model, which is based on an earlier two-dimensional model, has been applied to turbulent, combustion systems, including pulverized-coal systems. It uses an Eulerian framework for the gas phase and a Lagrangian framework for the particles. The code assumes equilibrium gas-phase chemistry and couples the turbulent flow field with the chemical reactions by integrating the equations over a probability density function. The model uses advanced numerics and a differencing scheme capable of solving the large computational meshes required to simulate practical furnaces. Convective and radiative heat transfer are also modeled. Radiative heat transfer is modeled using the discrete ordinates method. The model has been evaluated by comparison of predictions with experimental data from a large-scale 85-ME_e coal-fired utility boiler. The data include furnace profile measurements obtained with intrusive and laser-based optical probes. These comparisons show qualitative agreement of model predictions with observed trends, and indicate that the model can be used to provide insights into boiler operation.

Introduction

Increased consumption of fossil fuels in recent years has resulted in a greater interest to improve energy utilization and reduce pollutant emissions from fossil fuel combustion systems. Computer simulations of combustion systems can give insights into the phenomena occurring inside combustion and flow systems and can be used as design and analysis tools to improve efficiency and reduce pollutant emissions. However, these simulations are very complex, not only due to the numerical issues associated with solving the necessary equations but also because of the problems associated with mathematically describing the important chemical and physical processes occurring in these systems. The computer models developed for this purpose must be validated to demonstrate that they can be used to represent the physical processes occurring in these systems. One of the best ways to validate these models is by comparing the model predictions with measured data from combustion facilities of several scale-sizes. Comparisons with test results also provide insights into physical phenomena that govern these systems. However, while comparisons with data for small-scale systems are more common, such comparisons with large-scale combustion facilities are seldom performed, because internal furnace profile measurements are difficult and expensive to obtain. Further, since little or no *in situ* profile data have been reported for large utility furnaces, no comparisons of combustion model predictions with such data have previously been located.

Comprehensive combustion models include the various submodels of the physical processes occurring in combustion systems, including gaseous fluid dynamics, homogeneous gas phase reactions, radiative and convective heat transfer, devolatilization, heterogeneous reactions, and particle motion. A three-dimensional model, PCGC-3 (pulverized coal gasification/combustion-3 dimensions), has been developed for use in simulating practical combustion facilities. It is a generalized code for simulation of steady-state, reacting, and nonreacting gaseous or particle-laden systems, with an emphasis on turbulent, pulverized-coal combustion systems. The model uses conventional numerical methods and a differencing scheme for a completely arbitrary mesh and can solve the large computational meshes required for simulating practical furnaces. The model has been evaluated by new comparisons of code predictions with experimental profile data from inside a 85-MW_e coal-fired utility boiler.

Previous Work

Work in the area of comprehensive combustion modeling has been published or reviewed by numerous investigators.[1-9] Lockwood and Syed[1] discuss the capabilities and limitations of combustion modeling, and outline

* Author for correspondence. Phone: (801) 378-4024. Fax: (801) 378-3831.
† Research, Associate, ACERC.
‡ Dean, Engineering and Technology, and Director, ACERC.
• Abstract published in *Advance ACS Abstracts*, October 15, 1993.

(1) Lockwood, F. C.; Syed, S. A. *Combust. Sci. Technol.* **1979**, *19*, 129.
(2) Truelove, J. S. *Twentieth Symposium (International) on Combustion*; The Combustion Institute: Pittsburgh, PA, 1984; p 523.
(3) Truelove, J. S.; Holcombe, D. *Twenty-Third Symposium (International) on Combustion*; The Combustion Institute: Pittsburgh, PA, 1990; p 963.
(4) Smoot, L. D.; Smith, P. J. *ASME/JSME Thermal Engineering Joint Conference*; American Society of Mechanical Engineers: Honolulu, HI, 1987.
(5) Oran, E. S.; Boris, J. P. *Prog. Energy Combust. Sci.* **1981**, *1*, 1072.
(6) Gillis, P. A.; Smith, P. J. *Twenty-Third Symposium (International) on Combustion*; The Combustion Institute: Pittsburgh, PA, 1990; p 981.
(7) McDonald, H. *Prog. Energy Combust. Sci.* **1979**, *5*, 97.
(8) Westbrook, C.; Dryer, F. *Eighteenth Symposium (International) on Combustion*; The Combustion Institute: Pittsburgh, PA, 1981; p 749.
(9) Brewster, S.; Hill, S. C.; Radulovic, P. T.; Smoot, L. D. In Smoot, L. D., Ed.; *Fundamentals of Coal Combustion*; Elsevier: New York, 1993; Chapter 8.

0887-0624/93/2507-0874$04.00/0

Table I. Components in PCGC-3

process	description	references
gas fluid dynamics	Navier–Stokes equations	13, 14
	Newtonian fluid	
	Eulerian equations	
	Favre-averaged	
gas-phase chemistry	fast chemistry, mixing limited	15
	chemical equilibrium calculated by minimization of Gibbs free energy coupled with turbulence using probability density function (PDF), and mixture fractions	16, 17
turbulence	Prandtl mixing length	
	standard k–ϵ model	11
	nonlinear k–ϵ model	19
	adjusted for effects of particles	
radiation	Discrete-ordinates approach S4-24 directions	20, 21
devolatilization	two-step model	22
	Ubhayakar constants	23
	particle swelling allowed	
char oxidation	first-order reactions	13
	CO is primary product	
particle mechanics	PSI-CELL approach	24
	Langrangian equations	
	particle dispersion based on particle drag and gas turbulence	19
solution technique	SIMPLER, SIMPLEC, SIMPLEST TEACH method for differencing	25
	central and upwind finite-differencing	
NO_x formation	two fuel–NO mechanisms	26, 27
	thermal NO	
	global gas-phase reactions	
	heterogeneous NO reduction	

priorities for improvements. Truelove and Holcombe[2,3] discuss the theory and application of a similar two-dimensional model. Smoot and Smith[4] reviewed 3-D coal combustion models applied to furnaces. Oran and Boris[5] provide a general overview of different approaches to combustion modeling. Gillis and Smith[6] review recent three-dimensional models of gaseous and entrained-flow coal combustion. These models are similar in many ways to the model presented here, and the majority use variations of the SIMPLE algorithm[10] for coupling of the momentum and continuity equations, and the k–ϵ turbulence model[11]. However, simulation of practical combustion furnaces usually requires a large computational mesh to resolve the combustion details occurring inside these systems. Typically, three-dimensional simulations reported in the literature for large-scale systems use a relatively coarse computational grid and have not been validated by comparisons with experimental data due to the lack of data from large-scale systems. This work reports model predictions made with a relatively fine computational mesh and compares predictions with new measured profile data from a large-scale utility boiler. Point-for-point comparisons between predicted and measured data are shown, in contrast to comparisons with effluent data for previously reported work on large-scale, coal-fired systems.

Model Description

This combustion model is applicable to incompressible, steady-state gas and particle-laden flow and combustion processes, and was based on earlier foundations from a two-dimensional model[12,13], and a 3-D gaseous combustion model[6]. The various components used in PCGC-3 are summarized in Table I, which lists the process or submodel, a brief description, and several key references. These include gaseous flow, turbulence, particle flow, particle reactions, heat transfer and nitrogen-containing pollutants. The equations and submodels used as described in detail elsewhere[12,13], and only a brief description will be given here.

Gas Phase. The gas phase is described by elliptic, partial differential, conservation equations for a Newtonian fluid in either Cartesian or cylindrical coordinates. The gas-phase conservation equations are Favre-averaged and solved in the Eulerian framework, using a finite-difference formulation of the Navier-Stokes equations, coupled with the energy equation and the appropriate constitutive equations for the density and viscosity. Dilatation of the gas phase is neglected. A modified version of the TEACH[25] method is used for the irregular, finite-difference grid. Variations of the SIMPLE algorithm[10] are used for coupling the momentum and continuity equations. Differencing is performed using a combined weighted-central and hybrid upwind scheme. The finite difference equations are solved using an iterative line-by-line technique. Predicted quantities include the local velocity, temperature, density, and major species and pollutant concentrations. The particle phase equations are solved separately, and the two phases are coupled through various source terms.

Turbulence. The Reynolds stress terms, which result from Favre-averaging of the conservation equations, are approximated using the Boussinesq assumption and an effective eddy viscosity. The value of the eddy viscosity and subsequent closure of the equations can be made using either the Prandtl mixing length model, the standard two equation k–ϵ model[11], or the nonlinear k–ϵ model[18]. The k–ϵ model relates the turbulent kinetic energy, k, and its rate of dissipation, ϵ, using the Prandtl–Kolamagorov relationship to estimate the eddy diffusivity. The nonlinear k–ϵ model represents the Reynolds stress tensor as a nonlinear expansion of the Boussinesq hypothesis and retains several nonlinear terms that are neglected in the

(10) Pantakar, S. V. *Numerical Heat Transfer and Fluid Flow, Computation Methods in Mechanics and Thermal Sciences*; Hemisphere Publishing Corp.: Washington, DC, 1980.
(11) Launder, B. E.; Spalding, B. *Mathematical Models of Turbulence*; Academic Press: New York, 1972.
(12) Smith, P. J.; Fletcher, T. H.; Smoot, L. D. *Eighteenth Symposium (International) on Combustion*; The Combustion Institute: Pittsburgh, PA, 1979; p 1285.
(13) Smoot, L. D.; Smith, P. J. *Coal Combustion and Gasification*; Plenum Press: New York, 1985; p 77.

standard $k-\epsilon$ model. These nonlinear terms allow for more accurate representation of the normal Reynolds stress effects and prediction of secondary flow in noncircular ducts. PCGC-3 also includes a relaminarization model for low-Reynolds number flows.[28,29] This model modifies the $k-\epsilon$ model for better predictions with lower velocities in the near-wall region. The model is applicable to laminar, transitional, and fully turbulent flow regimes. The effects of the particles on the gas-phase turbulence are included using an empirical correlation based on the ratio of the bulk particle density and the gas density.

Fluctuations in the major field variables caused by the turbulence of the flow field can have a significant effect on the combustion reactions. PCGC-3 couples the effects of the turbulent flow field on the combustion chemistry by assuming that the gaseous reactions are limited by the mixing rates of reactants and not by the reaction kinetics. Thus, the gas-phase kinetics are assumed to be very fast relative to the time required for the fuel and oxidizer to mix at the molecular level. With this assumption, the gas composition can be calculated from local instantaneous equilibrium through minimization of the Gibbs free energy as a function of the local elemental composition and energy level. The local elemental composition is determined from the mixing of the inlet streams which is tracked using a conserved scalar called the mixture fraction (f). The mixture fraction is the ratio of the mass of gas from the primary stream to the total mass of gas at a given location, and is calculated from the solution of a partial differential mass conservation equation. Gas properties (i.e., density, temperature, species concentrations, etc.) and any other conserved scalars can be calculated from the local value of the mixture fraction.

The gas properties will fluctuate due to the turbulence, and the effect of these fluctuations on the combustion reactions is incorporated using a probability density function (PDF) which is calculated from the properties of the turbulent flow field. The local mean value of the mixture fraction, the local variance of the mixture fraction (g), and an assumed shape of the PDF[30] are required to calculate time-mean values of the gas properties. The local variance of the mixture fraction is calculated from a transport equation. The PDF has the form of a clipped Gaussian distribution, adjusted to account for turbulent intermittency[13].

The differential equation set used in PCGC-3 for cylindrical coordinates is shown in Table II. The generalized Cartesian equations can be obtained from the equations in Table II by equating the radius (r) with unity and neglecting several of the radial and tangential momentum source terms. This equation set includes the Navier–Stokes equations, the mixing equations for the inlet streams which include the mixture fraction (f) and the variance of the mixture fraction (g), the mixing equations for the coal off-gas which include the coal–gas mixture fraction (η) and the variance of the coal–gas mixture fraction (g_η) and transport equations for the turbulent kinetic energy (k), turbulent kinetic energy dissipation rate (ϵ), and the enthalpy (h). These are Eulerian, steady-state, second-order, nonlinear, elliptical, partial differential equations. The table shows the standard equation form characteristic of all equations and lists the source term for each of the different equations. The boundary conditions determine a unique solution for the equation set shown in Table II. Elliptic equations require that boundary conditions be specified at each boundary of the computational domain. Table III summarizes the boundary condition used on the various boundary surfaces for each of the variables in Table II.

Particle Flow. The particles are treated in a Lagrangian framework in which the particle field is represented as a series of trajectories through the gas continuum. Each trajectory has its own starting location and particle size and is representative of a large number of particles proportional to the total mass of particles. Particles can be reacting or nonreacting, and particle–particle interactions are neglected. The Lagrangian equations of continuity, momentum, and energy are used to calculate the particle properties and trajectories. These equations are shown in Table IV. Particle trajectories are tracked throughout the computational domain, and interactions between the particles and gas are incorporated by an exchange of source terms for mass, momentum, and energy. Turbulent particle dispersion is incorporated using an effective turbulent diffusivity based on experimental observations.

Particle Reactions. Particles are assumed to consist of coal, char, and ash. The particle reaction model describes the response of coal particles to their physical environment and is specific to coal combustion and gasification reactions. Coal devolatilization and char oxidation steps are included. Coal devolatilization is currently modeled by a simple, two-step mechanism[23], which produces an off-gas that reacts in the gas phase and a solid char. The off-gas from the coal is assumed to be of constant elemental composition. The gas formed from coal devolatilization participates in the gaseous reactions and is tracked with a coal–gas mixture fraction (η)[13], analogous to the gas-phase mixture fraction (f). The coal–gas mixture fraction is also calculated from a transport equation with a source term obtained from the Legrangian particle trajectories. The char reacts heterogeneously with various oxidizers (O_2, CO_2, H_2O) that diffuse to the particle surface. Coal reaction rates are characterized by first order, multiple, parallel reaction rates with fixed activation energies. Smith et al.[31] outline advanced methods for treating coal reaction processes based on coal structure that will be included in an improved version of this code.

Heat Transfer. PCGC-3 models convective, conductive and radiative heat transfer between the gases, particles and walls of the reactor. In coal furnaces, radiative heat transfer calculations are very complex, occurring in a multicomponent, nonuniform, emitting, absorbing, gas-particle systems, and the particles cause anisotropic scattering; the walls consist of nonuniform, emitting, reflecting, and absorbing surfaces. Radiative heat transfer is a dominant method of energy exchange in combustion furnaces, and is calculated based on an energy balance for a beam of radiation passing through a volume element containing an absorbing-emitting medium. The discrete-ordinates method[20,21] is used to model thermal radiation and predict incident and net radiative heat fluxes. This

(14) Crowe, C.; Smoot, L. D. In *Pulverized Coal Combustion and Gasification*; Smoot, L. D., Pratt, D. T., Ed.; Plenum Press, New York, 1979; Chapter 2.

(15) Pratt, D. T. In *Pulverized Coal Combustion and Gasification*; Smoot, L. D., Pratt, D. T., Eds.; Plenum Press, New York, 1979; Chapter 1.

(16) Kent, J. H.; Bilger, R. W. *Sixteenth Symposium (International) on Combustion*; The Combustion Institute: Pittsburgh, PA, 1977; p 1643.

(17) Lockwood, F. C.; Naguib, A. S. *Combust. Flame* **1975**, *24*, 109.

(18) Speziale, C. G. *J. Fluid Mech.* **1987**, *178*, 459.

Table II. Cylindrical Differential Equation Set

$$r\frac{\partial(\bar{\rho}\tilde{\phi})}{\partial x}+\frac{\partial(\bar{\rho}r\bar{v}\phi)}{\partial r}+\frac{\partial(\bar{\rho}\bar{w}\phi)}{\partial\theta}-r\frac{\partial}{\partial\theta}\left(\Gamma_\phi\frac{\partial\phi}{\partial x}\right)-\frac{\partial}{\partial r}\left(r\Gamma_\phi\frac{\partial\phi}{\partial r}\right)-\frac{\partial}{\partial\theta}\left(\frac{\Gamma_\phi\partial\phi}{r\ \partial\theta}\right)=S_\phi$$

equation	ϕ	Γ_ϕ	S_ϕ
continuity	1	0	S_p^m
X momentum	$\tilde{u}$	μ_e	$-r\frac{\partial p}{\partial r}+r\frac{\partial}{\partial x}\left(\mu_e\frac{\partial\tilde{u}}{\partial x}\right)+\frac{\partial}{\partial r}\left(\mu_e r\frac{\partial\bar{v}}{\partial x}\right)+\frac{\partial}{\partial\theta}\left(\mu_e\frac{\partial\bar{w}}{\partial x}\right)+r\bar{\rho}g_x-\frac{2}{3}r\bar{\rho}\tilde{k}+S_p^u+\tilde{u}S_p^m$
R momentum	$\tilde{\mu}$	μ_e	$-r\frac{\partial p}{\partial r}+\frac{\partial}{\partial x}\left(\mu_e\frac{\partial\tilde{u}}{\partial r}\right)+\frac{\partial}{\partial r}\left(\mu_e r\frac{\partial\bar{v}}{\partial r}\right)+\frac{\partial}{\partial\theta}\left(\mu_e\frac{\partial\bar{w}}{\partial r}-\frac{\tilde{w}}{r}\right)+S_p^v+\bar{v}S_p^m-\frac{2\mu_e\partial\bar{w}}{r\ \partial\theta}-\frac{2\mu_e\bar{v}}{r}+\bar{\rho}\tilde{w}^2+r\bar{\rho}g_r-\frac{2}{3}r\bar{\rho}\tilde{k}$
ϕ momentum	$\bar{w}$	μ_e	$-\frac{\partial p}{\partial\theta}+r\frac{\partial}{\partial x}\left(\frac{\mu_e\partial\tilde{u}}{r\ \partial\theta}\right)+\frac{\partial}{\partial r}\left(\mu_e\frac{\partial\bar{v}}{\partial\theta}-\mu_e\tilde{w}\right)-\bar{\rho}\bar{v}\tilde{w}+\frac{\partial}{\partial\theta}\left[\left(\frac{\mu_e}{r}\right)\left(\frac{\partial\bar{w}}{\partial\theta}+2\bar{v}\right)\right]\mu_e\left(\frac{\partial\bar{w}}{\partial r}+\frac{1}{r}\frac{\partial\bar{v}}{\partial\theta}-\frac{\tilde{w}}{r}\right)+r\bar{\rho}g_\theta-\frac{2}{3}r\bar{\rho}\tilde{k}+S_p^w+\tilde{w}S_p^m$
mixture fraction	$\tilde{f}$	$\frac{\mu_e}{\sigma_f}$	S_p^f
mixture fraction variance	$\tilde{g}$	$\frac{\mu_e}{\sigma_g}$	$r\left(\frac{C_{g1}\mu_e}{\sigma_g}\right)\left[\left(\frac{\partial\tilde{f}}{\partial x}\right)^2+\left(\frac{\partial\tilde{f}}{\partial r}\right)^2+\left(\frac{\partial\tilde{f}}{r\partial\theta}\right)^2\right]-C_{g2}r\bar{\rho}\tilde{g}\tilde{\epsilon}\tilde{k}$
enthalpy	$\tilde{h}$	$\frac{\mu_e}{\sigma_h}$	$\tilde{u}\frac{\partial p}{\partial x}+\bar{v}\frac{\partial p}{\partial r}+\bar{w}\frac{\partial p}{\partial\theta}+q'_{rg}+S_p^h+\tilde{h}S_p^m$
coal gas mixture fraction	$\tilde{\eta}$	$\frac{\mu_e}{\sigma_\eta}$	S_p^η
coal gas fraction variance	g_η	$\frac{\nu_e}{\sigma_{g\eta}}$	$r\left(\frac{C_{g1}\mu_e}{\sigma_{g\eta}}\right)\left[\left(\frac{\partial\tilde{\eta}}{\partial x}\right)^2+\left(\frac{\partial\eta}{\partial r}\right)^2+\left(\frac{\partial\eta}{\partial\theta}\right)^2\right]-\frac{C_{g2}\bar{\rho}\epsilon g_\eta}{k}$
turbulent energy	$\tilde{k}$	$\frac{\mu_e}{\sigma_k}$	$r(G-\overline{\rho\epsilon})$
dissipation rate	$\tilde{\epsilon}$	$\frac{\mu_e}{\sigma_\epsilon}$	$r(C_1G-C_2\bar{\rho}\tilde{\epsilon})\tilde{\epsilon}/\tilde{k}$

where

$$G=\mu_e\left\{2\left[\left(\frac{\partial\tilde{u}}{\partial x}\right)^2+\left(\frac{\partial\bar{v}}{\partial r}\right)^2+\left(\frac{1}{r}\frac{\partial\bar{w}}{\partial\theta}+\frac{\bar{v}}{r}\right)^2\right]+\left(\frac{\partial\tilde{u}}{\partial r}+\frac{\partial\bar{v}}{\partial x}\right)^2+\left(\frac{1}{r}\frac{\partial\tilde{u}}{\partial\theta}+\frac{\partial\bar{w}}{\partial x}\right)^2+\left(\frac{1}{r}\frac{\partial\bar{v}}{\partial\theta}+\frac{\partial\bar{w}}{\partial r}-\frac{\tilde{w}}{r^2}\right)^2\right\}$$

method solves the integro-differential, radiative transfer equation in a number of discrete, angular directions spanning the total solid angle. This results in a series of coupled, partial differential equations of radiation intensity which can be discretized using finite-difference techniques. The number of discrete directions and resulting equations depend on the order of the discrete-ordinates approximation. In this combustion model, the S_4 approximation is used, resulting in the calculation of radiation intensities in 24 discrete angular directions for each computational cell. This level of angular discretization has been shown to provide accurate results for a variety of combustion system[20,21]. Conductive and convective heat transfer between the gas and particle phases is also included.

Nitrogen Pollutants. PCGC-3 contains a submodel for prediction of nitrogen pollutant emissions from pulverized coal combustion systems[27,28]. This submodel has the capability of predicting both fuel and thermal NO_x formation. Description of this submodel and its appli-

(19) Melville, E. K.; Bray, N. C. *Int. J. Heat Mass Transfer* **1979**, *22*, 647.
(20) Fiveland, W. A. *Am. Soc. Mech. Eng./Heat Transfer Div.* **1987**, 9.
(21) Jamaluddin, A. S.; Smith, P. J. *Combust. Sci. Technol.* **1988**, *59*, 321.
(22) Kobayashi, H.; Howard, J. B.; Sarofim, A. F. *Eighteenth Symposium (International) on Combustion*; The Combustion Institute: Pittsburgh, PA, 1944; p 411.
(23) Ubhayaker, S. K.; Stickler, D. B.; von Rosenberg, C. W.; Gannon, R. E. *Sixteenth Symposium (International) on Combustion*; The Combustion Institute: Pittsburgh, PA, 1977; p 427.
(24) Crowe, C. T.; Sharma, M. P.; Stock, D. E. *Fluids Eng.* **1977**, *99*, 325.
(25) Gosman, A. D.; Pun, W. M. *Calculation Recirculating Flow* **1973**.

Table III. PCGC-3 Boundary Conditions

	$\tilde{u}$	$\tilde{v}$	$\tilde{w}$	$\tilde{h}$	$\tilde{k}$	$\tilde{\epsilon}$	g_i, g_a	$\tilde{f}$	$\tilde{\eta}$
primary jet	uniform at u_p or profile	0, or profile	0, or profile	uniform at h_p	primary turbulence intensity	from empirical correlations	0	specified in input data	0
secondary jet	uniform at u_s or profile	0, or profile	0, or profile	uniform at h_s	secondary turbulence intensity	from empirical correlations	0	specified in input data	0
symmetry axis	$u_{i,1,k} = u_{i,2,k}$	$v_{1,j,k} = v_{2,j,k}$	$w_{1,j,k} = w_{2,j,k}$	$\tilde{h}_{i,1,k} = h_{i,2,k}$	$k_{i,1,k} = k_{i,2,k}$	$\tilde{\epsilon}_{i,1,k} = \tilde{\epsilon}_{i,2,k}$	$g_{i,1,k} = g_{i,2,k}$	$\tilde{f}_{i,1,k} = \tilde{f}_{i,2,k}$	$\tilde{\eta}_{i,1,k} = \tilde{\eta}_{i,2,k}$
north wall	τ_w from wall function	0	τ_w from wall function	q_w from wall function	near wall values from wall function	near wall values from length scale	$g_{i,j,k} = g_{i,j-1}$	$\tilde{f}_{i,j,k} = \tilde{f}_{i,j-1,k}$	$\tilde{\eta}_{i,j,k} = \tilde{\eta}_{i,j-1,k}$
south wall	τ_w from wall function	0	τ_w from wall function	q_w from wall function	near wall values from wall function	near wall values from length scale	$g_{i,j,k} = g_{i,j+1}$	$\tilde{f}_{i,j,k} = \tilde{f}_{i,j+1,k}$	$\tilde{\eta}_{i,j,k} = \tilde{\eta}_{i,j+1,k}$
west wall	0	τ_w from wall function	τ_w from wall function	q_w from wall function	near wall values from wall function	near wall values from length scale	$g_{i,j,k} = g_{i+1,j,k}$	$\tilde{f}_{i,j,k} = \tilde{f}_{i+1,j,k}$	$\tilde{\eta}_{i,j,k} = \tilde{\eta}_{i+1,j,k}$
east wall	0	τ_w from wall function	τ_w from wall function	q_w from wall function	near wall values from wall function	near wall values from length scale	$g_{i,j,k} = g_{i-1,j,k}$	$\tilde{f}_{i,j,k} = \tilde{f}_{i-1,j,k}$	$\tilde{\eta}_{i,j,k} = \tilde{\eta}_{i-1,j,k}$
top wall	τ_w from wall function	τ_w from wall function	0	$h_{i,j,k} = h_{i,j,k-1}$	near wall values from wall function	near wall values from length scale	$g_{i,j,k} = g_{i,j,k-}$	$\tilde{f}_{i,j,k} = \tilde{f}_{i,j,k-1}$	$\tilde{\eta}_{i,j,k} = \tilde{\eta}_{i,j,k-1}$
bottom wall	τ_w from wall function	τ_w from wall function	0	$h_{i,j,k} = h_{i,j,k+1}$	near wall values from wall function	near wall values from length scale	$g_{i,j,k} = g_{i,j,k+}$	$\tilde{f}_{i,j,k} = \tilde{f}_{i,j,k+1}$	$\tilde{\eta}_{i,j,k} = \tilde{\eta}_{i,j,k+1}$
outlet	$\tilde{u}_{i,j,k} = \tilde{u}_{i-1,j,k}$	0	$\tilde{w}_{i,j,k} = \tilde{w}_{i-1,j,k}$	quadratic extrapolation	quadratic extrapolation	quadratic extrapolation	quadratic extrapolation	quadratic extrapolation	quadratic extrapolation

Table IV. Particle Phase Equations

momentum	$\alpha d\vec{v}_j/dt = \Gamma_d(\vec{v}_g - \vec{v}_j) + \alpha_j\vec{g}$
energy	$d(\alpha_j h_j)/dt = Qr_j - Q_j - r_j h_{jg}$
continuity	$d(\alpha_{ij})/dt = r_{ij}$

cation with PCGC-3 to predict NO_x emissions from a utility boiler are discussed in a companion paper[32].

Solution Technique. The partial differential equations in PCGC-3 are highly nonlinear and must be solved numerically. A combined, first-order upwind and weighted central-differencing scheme is used to discretize the differential equations. Simulation of utility furnace geometries can involve a wide disparity of grid sizes, and the differencing scheme has been formulated to minimize numerical diffusion and errors resulting from nonuniform grids.

The classical problem in computational fluid dynamics is the determination of the pressure field. Closure of the momentum equations can be obtained using the continuity equation; however, this is complicated by the fact that the pressure does not explicitly appear in the continuity equation. Solutions of the momentum and continuity equations of the velocity and the pressure field are coupled using variations of the SIMPLE (semi-implicit method for solving pressure limited equations) algorithm[10]. These approaches require an initial guess of the pressure and velocity fields, which are then updated through a series of corrections to the pressure and velocity fields.

Solution of the particle phase conservation equations is based on the PSI-CELL technique of Crowe et al.[24] This approach assumes that the particle phase is dispersed to the extent that particle–particle interactions can be neglected. Coupling between the gas and particle phases occurs through source terms that are calculated as the discrete particles pass through the volume elements of the gas flow field. This gas–particle coupling necessitates an iterative solution of gas and particle phases to achieve overall convergence. The gas flow field is first converged to a specified tolerance, and this solution is then used for the particle momentum, reaction, and energy calculations. The mass, momentum, and energy source terms resulting from the particle calculations are then used to update the gas-phase calculations. This process is repeated until overall convergence is achieved, as measured by the amount of change in the gas phase following a particle calculation.

Experimental Measurements

In situ measurements from a utility boiler[33-39] have recently been made for use in evaluating the combustion model, and for interpreting combustion processes. Measured quantities were

(26) Hill, S. C.; Smoot, L. D.; Smith, P. J. *Twentieth Symposium (International) on Combustion*; The Combustion Institute: Pittsburgh, PA, 1984; p 1391.
(27) Boardman, R. D. Ph.D. Dissertation, Brighan Young University, Provo, UT, 1990.
(28) Jones, W. P.; Launder, B. E. *Int. J. Heat Mass Transfer* **1972**, *15*, 301.
(29) Jones, W. P.; Launder, B. E. *Int. J. Heat Mass Transfer* **1973**, *16*, 1119.
(30) Bilger, R. W. In *Turbulent Flow with Nonpremixed Reactants*; Libby, P. A. Williams, F. A., Eds.; Turbulent Reacting Flows; Springer-Verlag: Berlin, 1980.
(31) Smith, K. L.; Smoot, L. D.; Fletcher, T. H. In *The Fundamentals of Coal Combustion*; Elsevier: The Netherlands, in press.
(32) Smoot, L. D.; Boardman, R. D.; Brewster, B. S.; Hill, S. C.; Foli, *Energy Fuels*, in this issue.
(33) Bonin, M. P.; Queiroz, M. *Combust. Flame* **1990**, *85*, 121.
(34) Butler, B. W.; Webb, B. W. *Heat Transfer in Combustion Systems*; *ASME/HTD* **1990**, *142*, 49.
(35) Butler, B. W.; Wilson, T.; Webb, B. W. *Twenty-fourth Symposium (International) on Combustion*; The Combustion Institute: Pittsburgh, PA, 1993; p 1333.

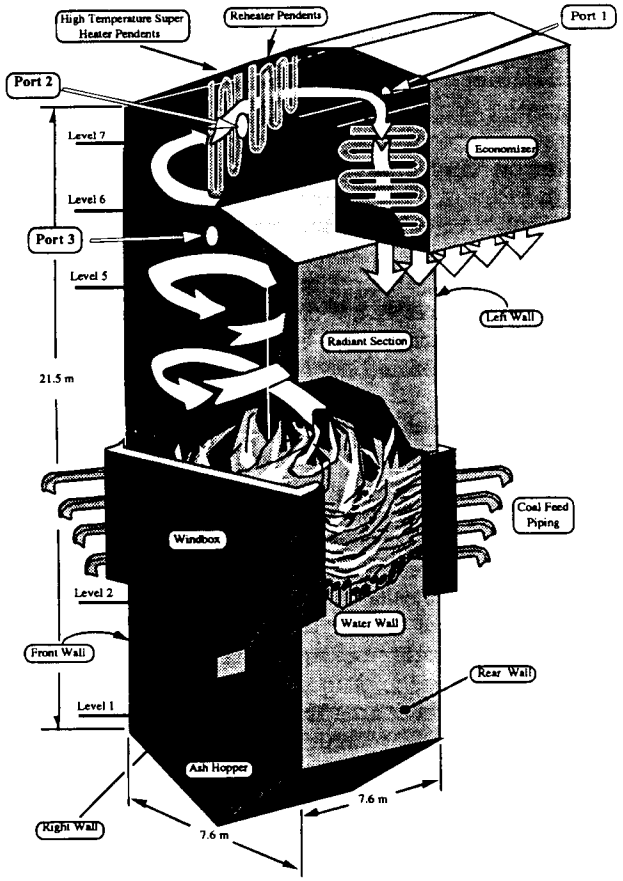

Figure 1. Artist's rendition of Goudey furnace (used with permission from Bonin and Queiroz[32]).

spatially resolved gas velocities, temperatures, and species concentrations, particle size distribution, particle velocities, particle number densities, and radiative heat fluxes. Test variables were coal type, particle size distribution, furnace load, burner tilt, and percent excess air. These measurements were made at the Goudey Station power plant in Johnson City, NY, which is operated by New York State Electric and Gas Co. (NYSEG). Two sets of tests were made, the first during the summer of 1989 and the second in the summer of 1991. The tests discussed in this paper were made during the summer of 1991. The furnace is a tangentially-fired, forced-recirculation, pulverized coal unit with an 85-ME_e electric capacity. A schematic of the furnace in Figure 1 shows the different regions of the furnace as well as the dimensions. Representation of the furnace walls is shown in Figure 2, which illustrates the locations and sizes of the various ports in the furnace. The boiler has seven access levels, six of which have ports available for data acquisition. The boiler has 16 corner burners, all of which were operational during the test series.

Most of the sampling probes were 3 m long, and the maximum probe insertion depth was approximately 2.5 m from the inner boiler wall due to the wall thickness and the port configuration. For the temperature measurements, the probe was 4 m long and could be inserted 3.2 m into the boiler, as measured from the inside wall. Gas temperatures were measured using a triply-shielded, water-cooled suction pyrometer. Repeated temperature measurements at the same conditions showed reproducibility of

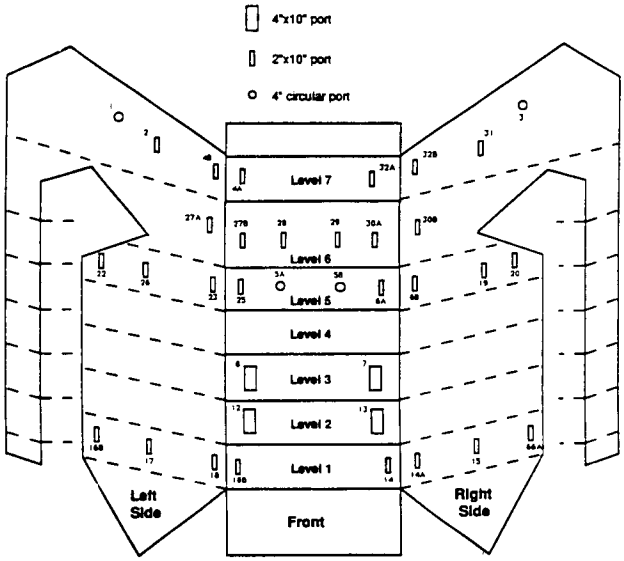

Figure 2. Port locations in the Goudey furnace.

about ±30 K. Most measurements were made with the probe normal to the furnace wall. Total incident radiant flux was measured with a water-cooled, wide angle, ellipsoidal radiometer. A water-cooled, dusty pitot tube was used for velocity measurements. On-line O_2 measurements were made, but all other gas composition measurements were made from stored gas samples. A laser-based, water-cooled, particle counter-sizer-velocimeter (PCSV) was used for measuring local number densities, particle sizes, and velocities. Access ports were available at levels 2, 3, 5, 6, and 7 (see Figures 1 and 2) through 2 in. × 10 in. corner ports, 4 in. circular ports, or 4 in. × 10 in. burner ports. Typically, each test lasted 2 h during which conditions were held steady with no wall or soot blower operations. One 24-h baseline test was conducted with measurements made at different ports. Repeatability tests were made for several test variables, which indicated that boiler operation was relatively steady during the tests.

Furnace Simulations

Simulations of the Goudey furnace have been performed for two test cases with different coals. Simulation of practical furnaces requires a large computational mesh to identify the processes occurring inside of these systems, particularly in the near-burner region. Gillis and Smith[6] showed for similar tangential- and wall-fired boilers that in excess of 200 000 cells were required to have grid-independence with a gaseous combustion case. Their study was used as a guide in constructing the computational mesh for this case. Also, simulations of this furnace have been made with three different computational meshes of 37 632 (28 × 28 × 48), 85 500 (30 × 30 × 95), and 240 100 (49 × 49 × 100) cells to determine the grid size required to achieve grid-independence for this geometry. Grid-independence was verified by visually comparing plots of several predicted quantities from cases with the same input conditions but different computational grids. If grid-independence has not been attained, the predicted quantities can show considerable differences for the same set of conditions[6]. Simulations were also performed assuming symmetry of the furnace, for only half of the furnace using 122 500 (25 × 49 × 100) computational cells. This mesh was used in the simulations discussed in this paper. The model calculations use a completely arbitrary grid spacing, which allows for the computational mesh to be concentrated in the regions of large gradients (i.e., near the burner region).

(36) Huntsman, L. K. M.S. Thesis, Brigham Young University, Provo, UT, 1990.
(37) Cannon, J. N.; Webb, B. W.; Queiroz, M. *Fossil Fuel Combust., ASME* **1991**, *33*, 49.
(38) Butler, B. W. Ph.D. Dissertation, Brigham Young University, Provo, UT, 1992.
(39) Oettli, M. C. M.S. Thesis, Brigham Young University, Provo, UT, 1993.

Table V. Operating Conditions and Coal Characteristics for the Goudey Furanace Tests

	test 4	test 5
gross power (MW_e)	85	82
excess air (%)	4.5	4.4
air flow rate (kg/h)	487,400	463,700
coal feed rate (kg/h)	29,100	28,350
measurement ports	3, 5a, 7, 64	3, 5a, 7, 64

	coal 1		coal 2	
	as received %	dry %	as received %	dry %
moisture	5.16	–	5.82	–
volatile matter	35.03	36.93	20.01	21.24
fixed carbon	52.32	55.09	64.09	68.0
ash	7.57	7.98	10.08	10.70
sulfur	2.07	2.18	1.47	1.56
carbon	76.71	80.87	73.59	78.14
hydrogen	3.29	3.47	4.30	4.56
nitrogen	1.14	1.20	1.01	1.07
oxygen	4.06	4.30	3.73	3.97
heating value (kJ/kg)	30 690	32 350	30 290	32 160
mass mean diameter (μm)	31		18	
hargrove grindability index	59		90	

The simulations were performed on a IBM RS/6000-550 superworkstation computer with 512 MB of main memory, and a Convex 220 minisupercomputer with 256 MB of main memory. The CPU time required for these coupled gas–particle simulations varied between 30 and 60 h for convergence. The simulations were accomplished by first calculating the gas phase for a fixed number of iterations and then performing the particle calculations for each of the particle trjectories. The source terms for the gas-phase equations were then updated based on the particle calculations, and the gas phase was again calculated for a fixed number of iterations. This cycle was repeated until the gas phase did not change significantly following the particle calculations.

Two cases from the 1991 Goudey tests were simulated. The tests (4 and 5) had similar operating conditions and varied mainly in the coal type used. The operating conditions and coal characteristics for the two cases are summarized in Table V. The coal used in test 4 had a higher volatiles content (37 versus 21%, dry) and a larger mass mean particle diameter (31 versus 18 μm). Variations in the coal properties during the test runs were found to be negligible. The input conditions used with PCGC-3 for the simulations of tests 4 and 5 are shown in Table VI. The primary streams carried the coal into the furnace through the 16 coal burners. The flowrates shown are total flow rates into the furnace for all 16 burners. The coal burners were surrounded by the secondary streams which carried the remaining combustion air into the furnace. There was no coal in the secondary streams.

No information on wall temperatures in the Goudey furnace was available for these tests. PCGC-3 has three options related to the thermal boundary conditions: (1) energy equation with constant wall temperature, (2) energy equation with variable wall temperatures, and (3) specified heat loss throughout the furnace. Since detailed measurements of radiant wall heat fluxes were available for these tests[34], option 3 was used for these simulations, which still required coupled solution of the energy equation. Calculations are planned using option 2 for comparison with the simulations reported here. The calculations using

Table VI. PCGC-3 Input Conditions

	test 4	test 5
primary stream		
total flow rate (kg/s)	10.6	10.6
temperature (K)	360	360
mass fraction		
O_2	0.209	0.209
N_2	0.719	0.719
coal loading (kg/kg of gas)	0.50	0.50
secondary stream		
gas flow rate (kg/s)	57.1	57.1
temperature (K)	540	540
swirl no.	0.0	0.0
mass fraction		
O_2	0.209	0.209
N_2	0.719	0.719
coal particle density (kg/m^3)	1340	1340
particle size distribution	10.0 μm, 5%	2 μm, 5%
	20.0 μm, 25%	10 μm, 25%
	31.0 μm, 50%	18 μm, 50%
	45.0 μm, 15%	30 μm, 15%
	65.0 μm, 5%	38 μm, 5%
mass mean particle diameter, μm	31	18

variable wall temperatures will involve making an estimate of the wall temperature in different regions of the furnace based on gas temperatures and ash fouling of walls[40]. The basis for estimation of the heat loss used in these simulations is described below.

The central purpose of these boilers is to transfer the combustion energy to the water walls. Peak combustion temperatures are in the range of 1900 K in the burner zone and 1200 K toward the top of the furnace before the superheater and convective zones. Test results of Butler and Webb[34] show radiant wall heat fluxes in the range of 300–500 kW/m^2 in the lower furnace regions and 100–300 kW/m^2 in the upper region. Based on an average wall radiant heat flux of 250 kW/m^2 for a furnace of 25 m × 7.7 m × 7.5 m (see Figure 8 of Butler and Webb[34]), the incident radiant wall heat flux is in the range of 170 MW (90% effective water–wall surface area), or about $^2/_3$ of the total heat of combustion of the feed coal. Butler and Webb[34] report a wall emittance of 0.77 which further suggests an absorbed energy flux of (0.77 × $^2/_3$) about 50% of the combustion energy lost toward the furnace top. This estimated heat loss value is thus consistent with both wall heat flux and temperature measurements and was used in the computations. The heat loss value in the lower region is less and an estimated value of $^1/_3$ was used there.

For the particle calculations, 144 starting locations were used with 5 particle sizes at each starting location for a total of 720 particle trajectories. The particle sizes and mass fraction of each size used in these simulations are shown in Table VI. These particle size distributions were selected by fitting the measured mass mean and particle size distribution for the two coals. Since only half of the furnace was modeled (symmetry assumption), only eight coal burners were included in the calculation. Equal quantities of particles were injected in all eight burners. Calculations showed that smaller particles tended to more closely follow the gas flow and are more dispersed throughout the boiler. A given particle size can follow very different trajectories starting from only slightly different starting locations. Predicted coal devolatilization is completed very rapidly following particle heat-up, while char oxidation proceeds at a slower rate, but also is essentially completed in the burner region of the furnace

(40) Benson, S. A.; Jones, M. L.; Harb, L. N. In *Fundamentals of Coal Combustion*; Smoot, L. D., Ed.; Elsevier: New York, 1993; Chapter 4.

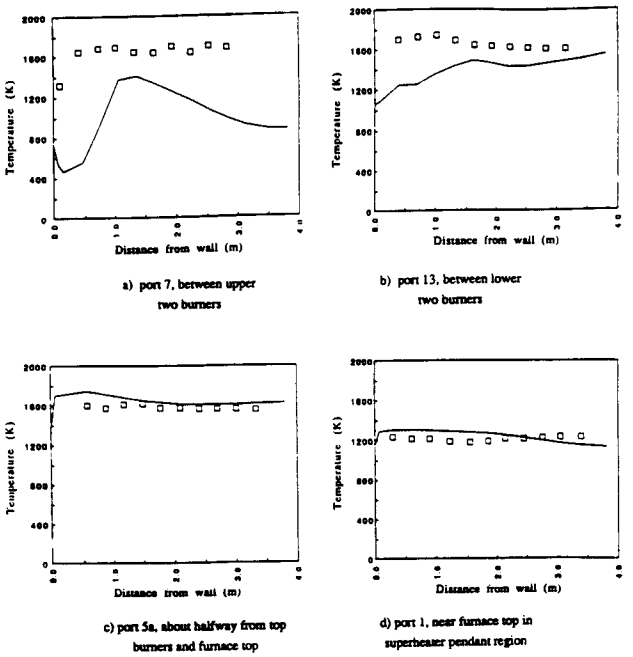

Figure 3. Comparisons of measured (□) and predicted (—) gas temperatures at four locations for test 4 in the Goudey furnace fired with coal 1.

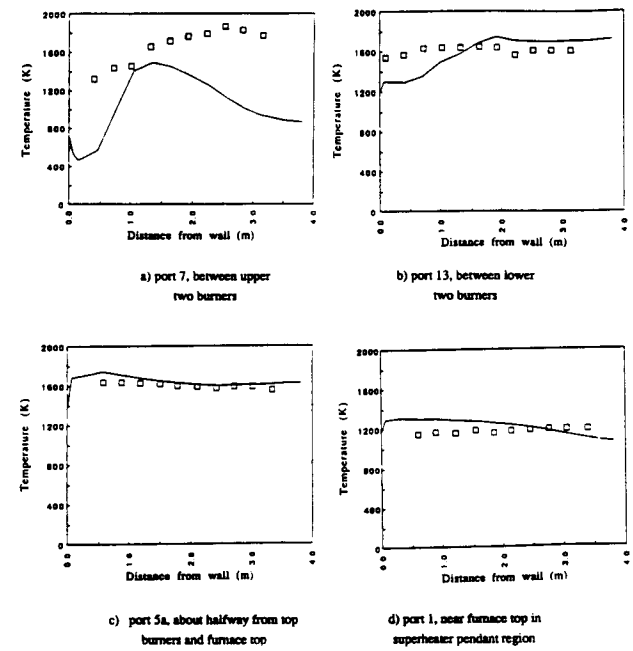

Figure 4. Comparisons of measured (□) and predicted (—) gas temperatures at four locations for test 5 in the Goudey furnace fired with coal 2.

even for the largest particles of 65 μm. In addition, the particles are predicted to collide with the walls on both sides of the furnace. Predictions provide useful insight into fouling and slagging behavior of coal mineral matter. The particle trajectories further illustrated the swirling nature of the particulate flow in the furnace, after the manner of the gaseous flow.

Figure 3 shows comparisons of measured and predicted gas temperatures at various port locations for test 4. Figure 4 shows similar comparisons for test 5. These figures show gas temperature as a function of distance from the wall of the furnace. Figure 3a compares temperatures as port 7, which is located between the upper two burners (there are four burners in each corner) on the front wall,

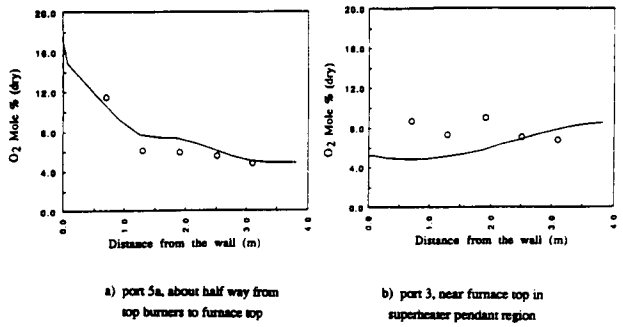

Figure 5. Comparisons of measured (O) and predicted (—) oxygen mole percent concentrations (dry) for test 4 in the Goudey furnace fired with coal 1 at two locations.

approximately 1.4 m from the right wall of the furnace. These temperatures are in the near-burner region of the combustion zone. The measured temperatures are much more uniform than the predicted values in this region, and the predicted values are consistently lower than the measured temperatures. Since these temperatures are in the near-burner region, this indicates that the code is predicting slower heat-up and burning of the coal particles than is observed in the furnace. Predicting the correct ignition location is a common problem in coal flames. Figure 3b compares temperatures as port 13, which is located directly below port 7 between the lower two burners in that corner. Similar to the temperatures at port 7, the predicted temperatures are consistently lower than the measured temperatures, and probably for the same reasons as discussed above.

Figure 3c compares temperatures at port 5a, which is located on the front wall of the furnace about half way between the top of the burners and the top of the furnace. Agreement between measured and predicted temperatures is quite good, with the largest discrepancies occurring near the furnace wall. This suggests that some of the boundary conditions used in the code require additional investigation. Predicted temperatures are slightly overpredicted in this region of the furnace. Figure 3d compares temperatures at port 1, which is located on the left wall near the top of the furnace in the superheater pendant zone. The magnitude of the measure and predicted temperatures agree quite well.

Figure 4 shows comparisons of measured and predicted gas temperatures at various port locations for test 5. Figure 4a compares temperatures at port 7, which corresponds to Figure 3a for test 4. This figure shows similar trends to those observed in test 4 and confirms the observation made previously that the model does not predict the exact ignition point. Figure 4b compares temperatures at port 13 and corresponds to Figure 3a for test 4. Figure 4b shows a similar trend to that observed in test 4, although the predicted temperature reaches a higher value and exceeds the measured values near the center of the furnace. Figure 4c compares temperatures at port 5a, which corresponds to Figure 3c for test 4. As with test 4, agreement is very good in this region of the furnace, with small discrepancies occurring near the furnace wall. Figure 4d compares temperatures at port 1, which corresponds to Figure 3d for test 4. The predicted temperatures are similar to those predicted for test 4, although the measured temperatures in test 5 are somewhat lower, especially near the wall. This results in a larger discrepancy between the measured and predicted temperatures near the wall.

Figure 5 shows comparisons of measured and predicted

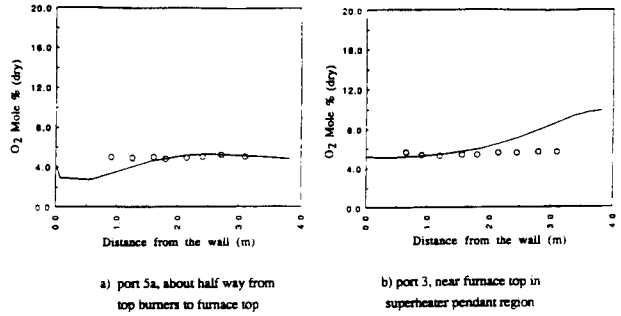

Figure 6. Comparisons of measured (○) and predicted (—) oxygen mole percent concentrations (dry) for test 5 in the Goudey furnace at two locations.

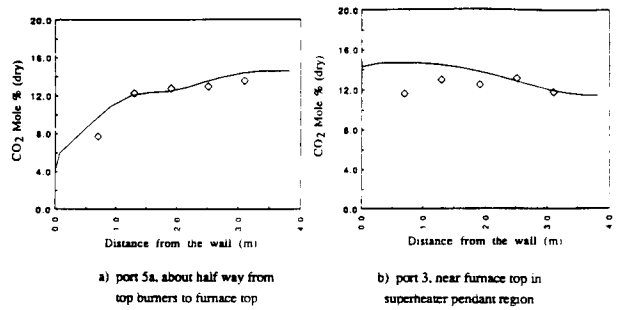

Figure 7. Comparisons of measured (◇) and predicted (—) CO_2 mole percent concentrations (dry) for test 4 in the Goudey furnace fired with coal 1 at two locations.

oxygen concentrations (dry) at two port locations for test 4. These figures show mole percent oxygen concentrations as a function of distance from the furnace wall. Figure 5a compares oxygen concentrations at port 5a. Agreement between measured and predicted values is excellent in this region of the furnace. Agreement of measured and predicted temperatures (Figure 3c) was also very good in this region. Figure 5b compares oxygen concentrations at port 3, which is located on the right wall near the top of the furnace in the superheater pendants, directly across from port 1. This figure shows that the model generally underpredicts the oxygen concentration in this region of the furnace, especially near the wall of the furnace.

Figure 6 shows comparisons of measured and predicted oxygen concentrations (dry) at two port locations for test 5. Figure 6a compares oxygen concentrations at port 5a. Agreement between measured and predicted values is very good in this region, especially away from the wall of the furnace. The largest discrepancies occur toward the furnace wall, although there are no measured values within 0.8 m of the wall. Figure 6b compares oxygen concentrations at port 3. Agreement between measured and predicted concentrations is quite good in this region, although the model overpredicts the oxygen concentrations near the center of the furnace.

Figure 7 shows comparisons of measured and predicted CO_2 concentrations at two port locations for test 4. These figures show mole percent CO_2 concentrations as a function of distance from the furnace wall. Figure 7a compares CO_2 concentrations at port 5a. Agreement between measured and predicted values is excellent in this region of the furnace. Agreement of measured and predicted temperatures (Figure 3c) and oxygen concentrations (Figure 5a) is also very good in this region of the furnace. Figure 7b compares oxygen concentrations at port 3. This figure shows that the model generally overpredicts the CO_2 concentration in this region of the furnace, especially

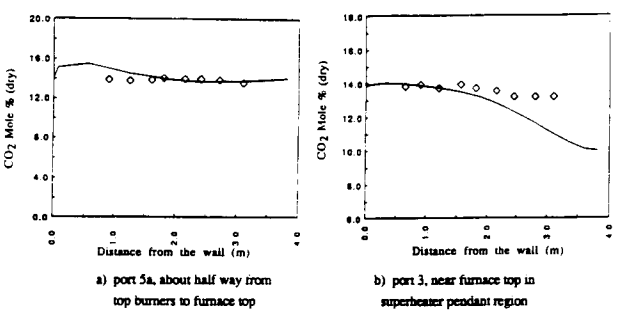

Figure 8. Comparisons of measured (◇) and predicted (—) CO_2 mole percent concentrations (dry) for test 5 in the Goudey furnace fired with coal 2 at two locations.

near the wall of the furnace. This is consistent with the predicted oxygen concentrations in this region and indicates that the model may be predicting a higher rate of combustion in this region.

Figure 8 shows a comparison of measured and predicted CO_2 concentrations for test 5 at two port locations. Figure 8a compares CO_2 concentrations at port 5a. Agreement between measured and predicted values is excellent in this region of the furnace. Figure 8b compares CO_2 concentrations at port 3. Agreement between measured and predicted values is very good in this region, with the largest discrepancies occurring near the center of the furnace.

Measured temperatures for coals 1 and 2 (test 4 versus test 5) are comparable except in the near-burner region (Figure 3a) where coal 1 produced higher temperatures in this region, presumably due to earlier ignition. This is consistent with the higher volatiles content of coal 1. The larger mean particle size for coal 1 should have little effect on devolatilization, since both coals had very small particles which heat very rapidly. Unlike temperatures, measured O_2 and CO_2 concentrations differ significantly between the two coals, particularly at port 5a. Coal 1 shows higher O_2 and lower CO_2 concentrations near the wall, which differences were reliably predicted by the model.

Several general observations can be made from the comparisons of the measured and predicted values shown for temperatures, oxygen and CO_2 concentrations. The model predictions show more structure thoughout the furnace than the measured values. The model does not correctly predict the exact location of ignition, which results in large discrepancies between measured and predicted values in the near-burner region. In regions of strong gradient, small uncertainities in probe position could also account for observed differences. Nevertheless, the predicted values show very good agreement with measured values downstream of the burner zone. Finally, the largest discrepancies between the measured and predicted values seem to generally occur near the wall of the furnace. This seems to indicate that the model shows more sensitivity to wall effects than physically occurs in the furnace. This may partially be explained by the increased difficulty of obtaining accurate measurements closer to the walls. But there are also numerical and theoretical difficulties associated with modeling the near-wall region, and these comparisons indicate that the treatment of the various boundary conditions may require further investigation.

Conclusions

A generalized, three-dimensional combustion model has been developed to simulate large-scale, steady-state,

particle-laden, reacting and nonreacting systems. The model uses an Eulerian framework for the gas phase, and a Lagrangian framework for the particles. The code uses conventional numerical methods and a flexible differencing scheme capable of solving large computational meshes. The model has been applied to data obtained by intrusive and nonintrusive probe methods in an 85-MW_e coal-fired utility boiler. Comparisons indicate that the model represents the qualitative trends observed in the furnace, except in the burner and near-wall regions where further work is required. Measured and predicted temperatures and species concentrations were in good agreement in most regions of the furnace, especially above the main combustion zone. The model was also able to predict some of the observed effects of coal type. Predicted particle trajectories in a turbulent environmental revealed valuable insights about the importance of particle starting locations and interactions with the boiler walls. The authors caution that the 3-D computations shown herein are among the first with coal to be obtained from this model and among the first such comparisons of measured profiles of temperature and gas composition from within a full-scale utility furnace. Since the accuracy of such comprehensive numerical solutions cannot be explicitly verified analytically, there may be some uncertainty in these results.

Acknowledgment. This work was funded principally by the Advanced Combustion Engineering Research Center (ACERC) at Brigham Young University. ACERC receives funds from the National Science Foundation's Engineering Centers Division, the State of Utah, Brigham Young University, and 31 industrial and governmental participants. Financial and technical support was also received for the utility boiler tests from the Empire State Electric Energy Research Corp. (ESEERCO) and New York State Electric and Gas Co. (NYSEG). Drs. Andrew Eaton, Steven Barthleson, Augustine Foli, and Subrata Sen also made significant contributions in development of the 3-D model, as did Prof. Philip J. Smith (currently at the University of Utah) in previous years.

Nomenclature

c, C	constants
f	mixture fraction
g	gravitational acceleration, mean square fluctuation
h	enthalpy
k	kinetic energy of turbulence
p	pressure
PDF	probability density function
Q	heat-transfer rate
r	radial direction, reaction rate
S	source term
t	time
T	temperature
u	axial velocity component
v	velocity vector, radial velocity component
w	tangential velocity component
x	axial direction
Y	stoichiometric coefficient
α	mass, intermittency
ϵ	dissipation rate of turbulent energy
η	coal gas mixture fraction
Γ	turbulent diffusion coefficient
μ	viscosity
ν	eddy viscosity
ϕ	stoichiometric coefficient, solution variable
ρ	density
σ	turbulent Schmidt or Prandtl number
θ	angular direction

Subscripts and Superscripts

a	ash
b	bulk
c	convective, raw coal
d	diffusive
D	drag
e	eddy
f	mixture fraction
g	gas
h	enthalpy, char
i	intermittency of inlet fluid, coal component
j	particle type or size index
k	element
l	heterogeneous reaction index
L	Lagrangian
m	mass, reaction index
p	particle, primary
r	radiation
s	secondary
t	turbulent
u	due to axial velocity
x	axial direction
η	coal gas mixture fraction
μ	viscosity
$\rightarrow$	vector
$-$	Reynold's mean
$\cdot$	relaxation
$\sim$	Favre mean